J. Fluid Mech. (2005), *vol.* 545, *pp.* 329–338.
doi:10.1017/S0022112005007184 Printed in the United Kingdom

Retraction dynamics of aqueous drops upon impact on non-wetting surfaces

By DENIS BARTOLO[1], CHRISTOPHE JOSSERAND[2] AND DANIEL BONN[1,3]

[1]Laboratoire de Physique Statistique de l'ENS, 24 Rue Lhomond, 75231 Paris cedex 05, France

[2]Laboratoire de Modélisation en Mécanique, CNRS-UMR 7606, Case 162, 4 place Jussieu, 75252 Paris Cédex 05, France

[3]van der Waals-Zeeman Institute, University of Amsterdam, Valckenierstraat 65, 1018 XE Amsterdam, The Netherlands

(Received 26 July 2005 and in revised form 15 September 2005)

We study the impact and subsequent retraction of liquid droplets upon high-speed impact on hydrophobic surfaces. Extensive experiments show that the drop retraction rate is a material constant and does not depend on the impact velocity. We show that on increasing the Ohnesorge number, $Oh = \eta/\sqrt{\rho R_1 \gamma}$, the retraction, i.e. dewetting, dynamics crosses from a capillary–inertial regime to a capillary–viscous regime. We rationalize the experimental observations by a simple but robust semi-quantitative model for the solid–liquid contact line dynamics inspired by the standard theories for thin-film dewetting.

1. Introduction: drop impact on solid surfaces

Drops impacting onto solid surfaces are important for a large number of applications: for instance, almost all spray coating and deposition processes rely ultimately on the interaction of a droplet with a surface. A large variety of phenomena can be present during drop impact, from splashes to spreading, and from large wave surface deformation to rebound (see Rein 1993 and references therein).

Research on drop impact has a long history, starting with the pioneering studies of Worthington and later with the famous photographs of Edgerton (Worthington 1876; Edgerton & Killian 1954). Most previous work on drop impact has focused on determining the maximum diameter a drop can cover upon impact (Fukai *et al.* 1993; Roisman, Riboo & Tropea 2002; Clanet *et al.* 2004). However, the practical problem of deposition can be very different if one wants to efficiently deposit some material on the surface, especially when the surface is not wetted by the liquid, as is illustrated by the high-speed video pictures in figure 1 of the impact of a water droplet. The drop expands rapidly, due to the large speed with which it arrives at the surface. However, due to the hydrophobicity of the surface, subsequently the drop retracts violently, leading to the ejection of part of it from the surface: we observe droplet rebound. This 'rebound' it is the limiting factor for deposition in many applications, for instance for the deposition of pesticide solutions on hydrophobic plant leaves (Bergeron *et al.* 2000). We study here the impact and subsequent retraction of aqueous drops onto a hydrophobic surface, and seek to understand the dynamics of their expansion and retraction.

In general, these problems are difficult because for most practical and laboratory situations, three forces play an important role: the capillarity and viscous forces, and

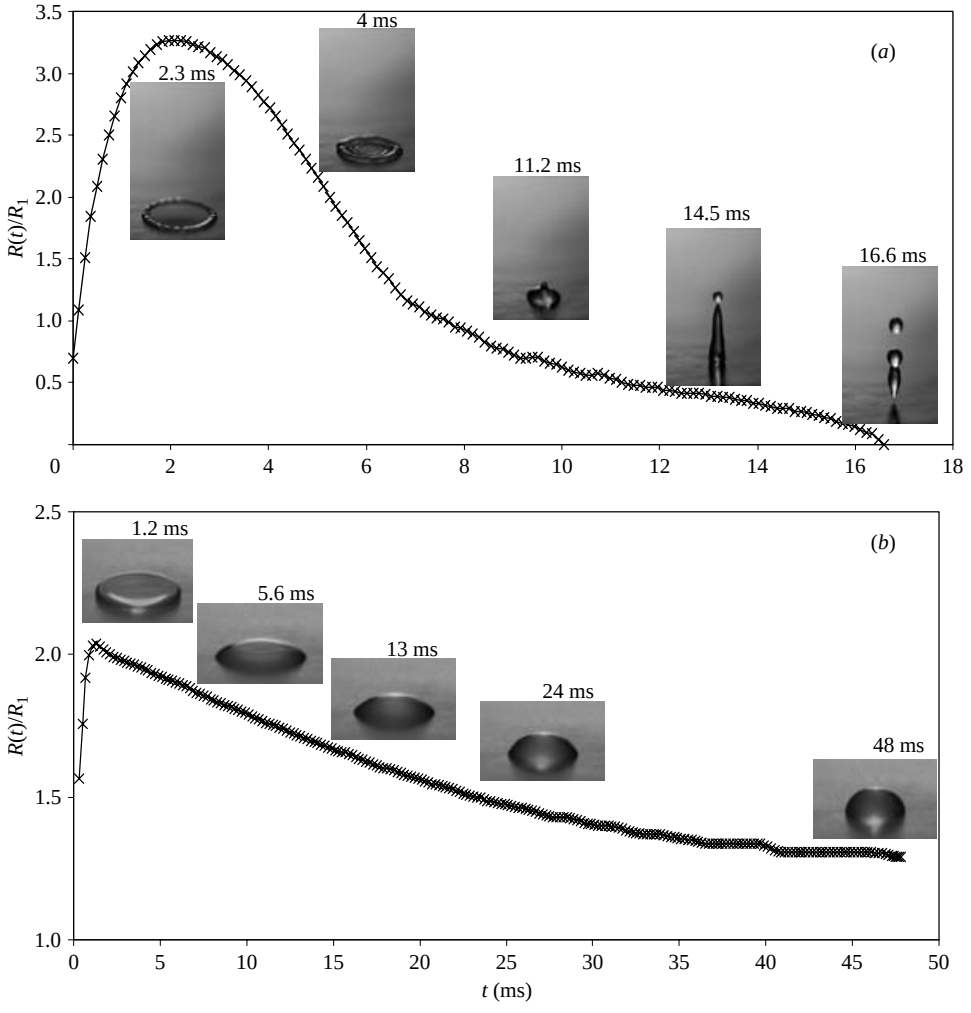

FIGURE 1. Temporal evolution of the contact radius of droplets upon impact and retraction, normalized by that of the spherical droplets before impact. The pictures show the shape of the droplets at the different stages of retraction. Droplet radius is 1 mm, impact speed is $2\,\mathrm{m\,s^{-1}}$: (*a*) pure water, (*b*) viscous water–glycerol mixture, viscosity 50 mPa s.

the inertia of the droplets. We try to disentangle the effects of the three forces here by performing systematic experiments, varying both the viscous and inertial forces. We provide experimental evidence for the existence of two distinct retraction regimes. In both, capillary forces are the motor behind the droplet retraction, which are, for the first regime countered by inertial forces. In the second regime the main force slowing the retraction is viscous. We also show that, perhaps surprisingly, the drop retraction rate (the retraction speed divided by the maximum radius) does not depend on the impact velocity for strong enough impacts. The dimensionless number that governs the retraction rate is found to be the Ohnesorge number, $Oh = \eta/\sqrt{\rho R_\mathrm{I}\gamma}$, with η the viscosity, ρ the liquid density, R_I the impacting drop radius, and γ the surface tension. The Ohnesorge number therefore compares the dissipative (viscous) forces to the non-dissipative (capillary and inertial) forces. The crossover between the two regimes is found to occur at a critical Ohnesorge number on the order of 0.05.

To develop a better understanding of the different regimes that are encountered, particularly the retraction dynamics in these regimes, we propose two simple hydrodynamic models inspired by the standard description of thin-film dewetting dynamics. These models provide a simple but quite robust picture that allows us to rationalize the retraction rate in both regimes. In order to consider the speed of retraction, one also needs to understand the maximum radius to which the droplet expands. Combining our results with those obtained by Clanet *et al.* (2004) for the maximum radius, we propose a phase diagram delimiting four regions for the spreading and retraction dynamics of impacting drops.

2. Drop retraction dynamics: generic features

As the impact dynamics of liquid droplets on a solid surface occurs usually in a few tens of milliseconds, we use a high-speed video system (1000 frames/second, Photonetics) to analyse the drop-impact events. When necessary, we use an ultra-high-speed system going up to 120 000 frames/second (Phantom V7). We study aqueous drops impacting on a solid surface; the surface we used is Parafilm, which is hydrophobic (receding contact angle for water $\theta_R \approx 80^\circ$). In addition, the surface has a low contact angle hysteresis with water, and allows us to obtain highly reproducible results. The liquids used are different water–glycerol mixtures. By varying the glycerol concentration, we vary the liquid viscosity, keeping the liquid density and its surface tension almost constant. For the highest concentration of glycerol, the surface tension has decreased from 72 (pure water) to 59 $\mathrm{mN\,m^{-1}}$, whereas the density has increased to 1150 $\mathrm{kg/m^{-3}}$. The viscosity is varied between 1 and 205 mPa s. Viscosity, density and surface tension were measured before each impact experiment. Drops were produced using precision needles, and their initial radius R_I was systematically measured on the images ($1.1 < R_I < 1.4$ mm). From the high-speed images such as shown in figure 1, we follow the contact radius R in time. This section summarizes the results of more than 80 different drop impact experiments, each of which was repeated at least two times.

Two series of experiments were performed: first, by letting the droplets fall from a fixed height, but increasing the viscosity, we increase the Ohnesorge number while keeping the inertial forces constant. The second series is performed at fixed viscosity and increasing the height from which the droplets falls; the droplet turns out to be in free fall (as is verified in the experiment to within a few percent) and so the relation between fall height h and impact velocity is simply $V_I = \sqrt{gh}$, with g the gravitational acceleration. Increasing the impact velocity increases the Weber number, *We*, keeping the Ohnesorge number fixed, where *We* compares the inertial forces to the capillary forces, $We \equiv \rho R_I V_I^2/\gamma$.

Here, we restrict considerations to high-speed impact conditions. More precisely, the Weber and Reynolds numbers are chosen so that $We > 10$ and $Re > 10$, where $Re \equiv \rho R_I V_I/\eta$ is the Reynolds number. This implies that inertial forces are at least one order of magnitude larger than both the capillary and the viscous forces. Such conditions imply large deformations of the drop when the liquid impinges on the solid substrate. On the other hand, we also restrain our experiments to impact speeds that are far from the 'splashing' regime in which the drop disintegrates after impact to form a collection of much smaller droplets (Mundo, Sommerfeld & Tropea 1995).

Figure 1 shows that two distinct regimes exist for the shape of the droplets after impact. For low fluid viscosity, we typically obtain the images shown in figure 1(*a*). At the onset of retraction, almost all of the fluid is contained in a donut-shaped rim, with

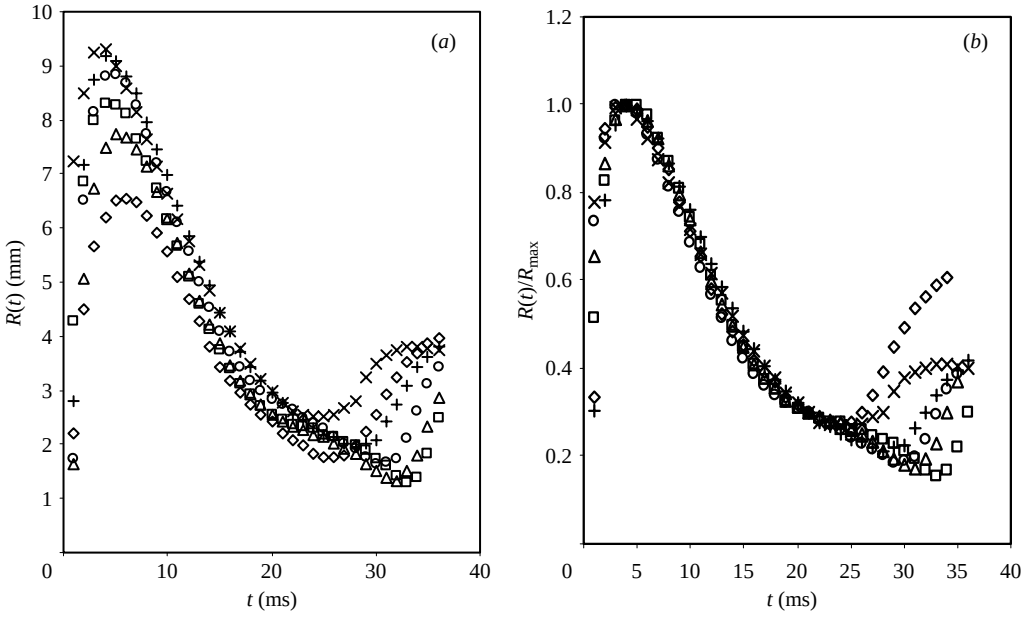

FIGURE 2. Temporal evolution of the contact radius for a water–glycerol drop $Oh = 9.1 \times 10^{-2}$, $R_I = 1.2$ mm: (*a*) contact radius vs. time, (*b*) contact radius normalized by the maximum spreading radius vs. time. Impact velocities: ×, $V_I = 2.4\,\mathrm{m\,s^{-1}}$; +, $V_I = 2.2\,\mathrm{m\,s^{-1}}$; ○, $V_I = 1.9\,\mathrm{m\,s^{-1}}$; □, $V_I = 1.7\,\mathrm{m\,s^{-1}}$; △, $V_I = 1.4\,\mathrm{m\,s^{-1}}$; ◇, $V_I = 1\,\mathrm{m\,s^{-1}}$.

only a thin film of liquid in the centre. For high viscosities the deformation of the drop is less important, and the pancake-shaped droplet of figure 1(*b*) results. These visual observations allow one to distinguish the capillary-inertial and the capillary-viscous regimes that are described in detail below.

2.1. *Drop retraction rate: influence of fall height and viscosity*

Figure 2 summarizes the most important findings of this study. The temporal evolution of the drop contact radius $R(t)$ for different impact velocities, shown in (*a*), is normalized in (*b*) by its maximal value at the end of the spreading R_{max}. Two important observations are made. (i) A well-defined retraction velocity V_{ret} can be extracted from each experiment; this is a non-trivial observation that will be rationalized below. (ii) Independently of the impact speed, all the $R(t)/R_{max}$ curves collapse onto a single curve for different impact velocities. Thus the retraction rate, rather than the retraction speed is the natural quantity to consider, and this rate is independent of the impact velocity. These results hold for all the viscosities tested in our experiments.

In figure 3 we plot the retraction rate $\dot{\epsilon} \equiv V_{ret}/R_{max}$ versus the impact Weber number, where V_{ret} is defined by $V_{ret} \equiv \max[-\dot{R}(t)]$. Clearly, the drop retraction rate does not depend on the impact velocity. One might think that the explanation for this observation is rather obvious: the initial kinetic energy of the droplet is transformed into surface energy (which fixes $R_{max}/RI \propto We^{1/2}$), and is then transformed back into kinetic energy (which in turn fixes $V_{ret} \propto V_I$). This naive explanation is wrong for the following reasons. First, it has been observed recently that, at the onset of retraction, low-viscosity liquids undergo vortical motion in the drop (Clanet *et al.* 2004). This residual flow in the drop reveals that part of the initial kinetic energy is still available, and thus that a simple energy balance argument cannot work. This was

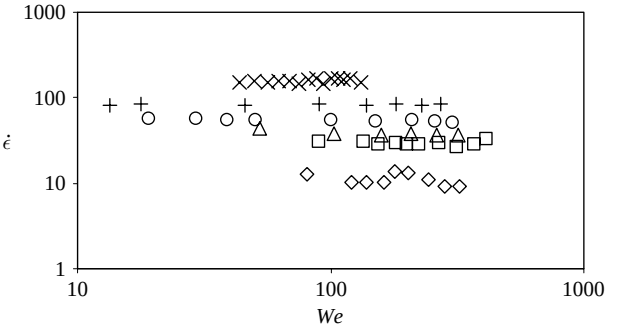

FIGURE 3. Retraction rate vs. Impact Weber number for various water–glycerol droplets. ×, $Oh = 2.5\times10^{-3}$; +, $Oh = 3.9\times10^{-3}$; ○, $Oh = 1.5\times10^{-2}$; △, $Oh = 1.6\times10^{-2}$; □, $Oh = 2.3\times10^{-2}$; ◇, $Oh = 7.1\times10^{-2}$.

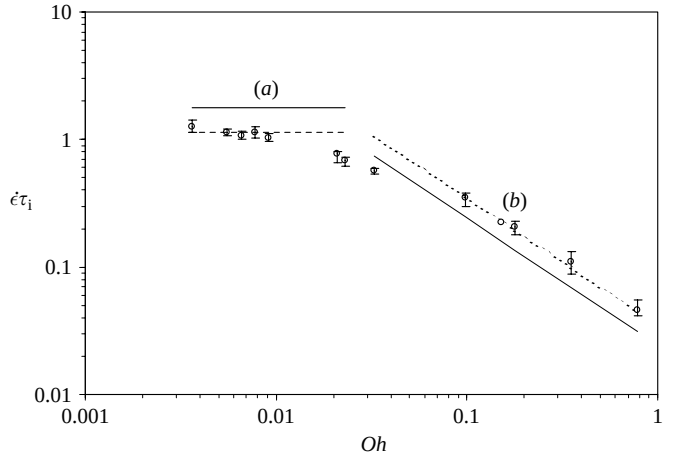

FIGURE 4. ○, Normalized retraction rate $\dot{\epsilon}\tau_i$ vs. the Ohnesorge number, experimental values. Error bars represent the maximum deviation from the mean value. Solid line: (*a*) $\dot{\epsilon}\tau_i$ evaluated using (3.2), (*b*) $\dot{\epsilon}\tau_i$ evaluated using (3.6). Dashed line: (*a*) fit obtained taking the mean value of the five first experimental points, (*b*) best fit according to the predicted $1/Oh$ power law.

indeed already suggested by previous observations of a clear disagreement between experiments and the $R_{max}/RI \propto We^{1/2}$ law (Fukai *et al.* 1993; Roisman *et al.* 2002; Okumura *et al.* 2003). The second reason follows directly from figure 3, where it is shown that the retraction rate depends on the viscosity and consequently that the previous inviscid picture is not correct.

We therefore performed experiments to elucidate the role of viscosity, or, equivalently, of the Ohnesorge number. It is convenient to define two intrinsic time scales for the droplet: viscous and inertial. The viscous time is the relaxation time of a large-scale deformation of a viscous drop: $\tau_v \equiv (\eta R_I)/\gamma$, whereas the inertial time scale: $\tau_i = (\frac{4}{3}\pi\rho R_I^3/\gamma)^{1/2}$ corresponds to the capillary oscillation period of a perturbed inviscid droplet. Since τ_i is independent of V_I and η, it is almost constant for all tested drops.

Figure 4 shows the retraction rate, made dimensionless using the inertial time, as a function of the Ohnesorge number. Two different regimes exist for the retraction rate. The first region where the retraction rate $\dot{\epsilon}$ is independent of the viscosity points

to an inertial regime and $\dot{\epsilon} \propto \tau_{\mathrm{i}}^{-1}$. The retraction rate is consequently found not to depend on the impact speed, a result similar to that obtained by Richard, Clanet & Quere (2002) who show that the contact time is independent of the impact speed. For higher viscosities, typically $Oh > 0.05$, the retraction rate decreases strongly. In this regime, capillary and viscous forces govern the dynamics: we find $\dot{\epsilon} \propto \tau_{\mathrm{v}}^{-1}$.

3. Two simple models for the drop retraction dynamics

We have established the existence of two different regimes for the retraction rate: a viscous one and an inertial one. We now develop some simple arguments allowing a semi-quantitative description of the dynamics, using ideas already existing for the dynamics of dewetting, a problem closely related to the current one.

3.1. *Inertial regime*

We employ a Taylor–Culick approach commonly used for the inertial dewetting of thin films (Taylor 1959; Culick 1960; Buguin, Vovelle & Brochard 1999) to describe the drop retraction rate. For high-velocity drop impact, liquid spreads out into a thin film of thickness h and radius $R_{\max}$. The liquid subsequently dewets the surface rapidly, and forms a rim that collects the liquid that is initially stored in the film. The shape of the drop surface is therefore never in a steady state and consists of a liquid film formed during the spreading stage and a receding rim. The contact angle at the outer side of the rim is taken to be very close to the receding contact angle (θ_{R}) since viscous effects can be neglected (Buguin *et al.* 1999). The dynamics is thus determined by a competition between capillary tension from the thin film and the inertia of the rim. We can write momentum conservation for the liquid rim as

$$\frac{\mathrm{d}}{\mathrm{d}t}\left(m\frac{\mathrm{d}R(t)}{\mathrm{d}t}\right) = F_{\mathrm{C}} \tag{3.1}$$

with m the mass of the liquid rim and F_{C} the capillary force acting on it, $F_{\mathrm{C}} \sim 2\pi\gamma R(t)\,[1-\cos(\theta_{\mathrm{R}})]$. The stationary solution of (3.1) can be obtained by writing $\dot{m}(t) = 2\pi\rho R V_{\mathrm{ret}} h$, and gives $V_{\mathrm{ret}} = \sqrt{\gamma\,[1-\cos(\theta_{\mathrm{R}})]/(\rho h)}$. Using volume conservation, $h \sim \frac{4}{3}R_1^3 R_{\max}^{-2}$, it follows that

$$\frac{V_{\mathrm{ret}}}{R_{\max}} \sim \tau_{\mathrm{i}}^{-1}\sqrt{\pi\,[1-\cos\theta_{\mathrm{R}})]} \tag{3.2}$$

which is the final result. Comparison with the experimental data shows that this equation not only gives the correct scaling behaviour for the retraction in this regime rate but also provides a rather accurate estimate of the numerical prefactor (see figure 4): the ratio between the experimental and predicted numerical prefactors is found to be 0.6. Repeating the experiment for water on a polycarbonate surface, which changes the contact angle value to 60°, we obtain exactly the same ratio of 0.6.

3.2. *Viscous regime*

At the opposite limit of very viscous liquids, the drops adopt pancake shapes upon impact. During the first stages of retraction, the pancake shape rapidly relaxes towards a roughly spherical cap, and remains like this during the retraction since the capillary number is small. During the retraction, only the contact angle varies slowly: it is mainly this slow contact angle dynamics that dictates the drop evolution during the retraction. Contrary to the previous analysis, the slow receding velocity allows us to assume a quasi-static dynamics for the surface shape during the retraction. In this

regime, it is then natural to assume that the work done by the capillary force F_C is dissipated through viscous flow near the contact line. Since we focus our study on high-speed impacts, R_{max} is always much larger that R_I which justifies a small-$\theta(t)$ approximation at the onset of retraction. The viscous effects near the contact line then lead to the well-known linear force–velocity relation (De Gennes 1985):

$$F_V = -\frac{6\pi\eta}{\theta}\ln\left(\frac{\Lambda}{\lambda}\right)R(t)\dot{R(t)} \tag{3.3}$$

where Λ and λ are respectively macroscopic and microscopic cutoff lengths. Λ is typically of the same order as the drop size $\sim 1\,\text{mm}$. λ is a microscopic length, and is usually taken to be of order $\lambda \sim 1\,\text{mm}$ (De Gennes 1985). On the other hand, the capillary force drives the retraction. Near the contact line it can be written:

$$F_C = 2\pi R(t)\gamma\,[\cos\theta(t) - \cos\theta_R]. \tag{3.4}$$

Volume conservation gives $\frac{4}{3}\pi RI^3 \sim \frac{1}{4}\pi\theta(t)R^3(t)$, where we have taken the small-angle limit. Equations (3.3) and (3.4) together with the volume constraint leads to the following relation for the variation of the contact radius:

$$\frac{\dot{R}(t)}{R(t)} = -\frac{\left[1 - \frac{1}{2}\theta^2(t) - \cos(\theta_R)\right]\theta(t)^{4/3}}{(144)^{1/3}\ln(\Lambda/\lambda)}\tau_v^{-1}, \tag{3.5}$$

obtained in the small-angle limit and only valid for short time after the onset of retraction. We estimate the retraction rate $\dot{\epsilon}$ as the maximum value of $\dot{R}(t)/R(t)$ so that

$$\frac{V_{ret}}{R_{max}} \approx \left(\frac{3}{25}\right)^{1/3}\frac{(1-\cos\theta_R)^{5/3}}{5\ln(\Lambda/\lambda)}\tau_v^{-1}. \tag{3.6}$$

Comparing again to the experiments, good agreement is found: the retraction rate is set solely by the viscous relaxation time τ_v and consequently $\dot{\epsilon}\tau_i \propto Oh^{-1}$. Beyond this correct scaling prediction, (3.6) provides a quite accurate estimate for the numerical prefactor as is shown in figure 4. Indeed, the ratio between the experimental and the predicted numerical prefactors is found to be 1.5. Again, repeating the experiment on a polycarbonate surface, this ratio changes only slightly from 1.5 to 1.8.

4. Conclusions and perspectives

Our experiments reveal that the drop retraction rate is independent of the impact speed. To account for the retraction speed, the maximum radius to which the droplet expands, must be known also. A number of studies have considered the maximum spreading radius (see for instance Fukai *et al.* 1993; Roisman *et al.* 2002; Clanet *et al.* 2004). However, no clear and unified picture emerges. An experimental study of R_{max}, combined with theoretical ideas in the same spirit as the ones presented here was done by Clanet *et al.* (2004). They obtain a zeroth-order (asymptotic) description of the spreading stage, compare it with experiments and suggest that two asymptotic regimes exist for R_{max}. The first is given by a subtle competition between the inertia of the droplet and the capillary forces; if only these two are important, it follows that $R_{max}/R_I \propto We^{1/4}$. In the second regime, R_{max} is given by a balance between inertia and viscous dissipation in the expanding droplet, leading to $R_{max}/R_I \propto Re^{1/5}$. Consequently, a single dimensionless number is defined that discriminates between the two regimes: $P = WeRe^{-4/5}$ referred to as the Impact number. The crossover between the two regimes occurs at P of order unity.

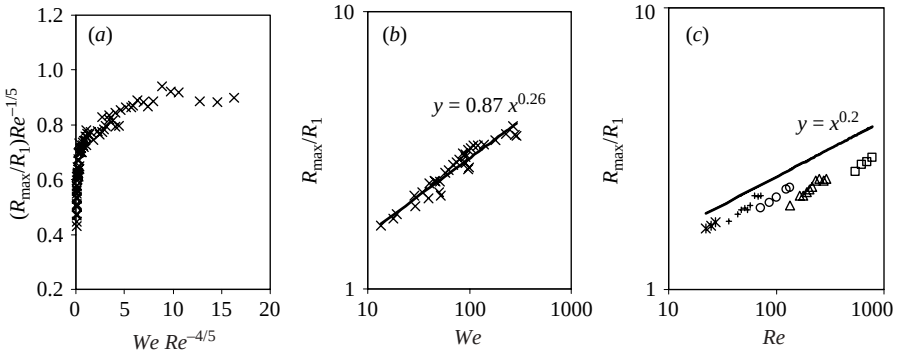

FIGURE 5. (*a*) Normalized maximum spreading radius vs. the impact number. (*b*) R_{max} (normalized by the radius before impact) vs. Weber number for small values of the impact number. Solid line: power-law fit. (*c*) R_{max} (normalized by the radius before impact) vs. Reynolds number for large values of the impact number. Solid line: predicted power-law dependence with power 0.2. *, $\eta = 10^{-1}$ Pa s; +, $\eta = 9.5 \times 10^{-2}$ Pa s; ○, $\eta = 4.8 \times 10^{-2}$ Pa s; △, $\eta = 2.8 \times 10^{-2}$ Pa s; □, $\eta = 10^{-2}$ Pa s.

Our experimental data are in qualitative agreement with their prediction, as is shown in figure 5(*a*) At low P, the scaling $R_{max}/R_I \sim We^{1/4}$ is clearly observed. However, for impacts corresponding to $P > 1$, we observe only a very slow variation of the maximum spreading radius as a function of P. Therefore, the relation between R_{max} and the Reynolds number is not very clear from our data (figure 5*c*). Although the main trend does not strongly contradict the prediction $R_{max}/R_I \propto Re^{1/5}$, a power-law fit of our data gives exponents that are always smaller than the predicted value of 0.2. Perhaps even more important – in view of the small range of the maximal expansion R_{max} that we cover – is that the different water–glycerol mixtures do not appear to collapse on a single curve, as would be predicted by the above argument. However, since the maximum value of P that we reach is of order 10, we not have reached the purely viscous regime. In that case, the capillary, inertial and viscous forces are still of comparable amplitude and have to be taken into account together. Note also that the more sophisticated models reviewed in Ukiwe & Kwok (2004) do not provide better agreement with our experimental measurements.

Despite this small problem, we are now able to develop a simple unified picture for drop impact dynamics accounting for both the spreading and the retraction dynamics. The two natural dimensionless numbers that have been identified are the impact number P, that quantifies the spreading of the droplet, and the Ohnesorge number Oh that quantifies the retraction. We can thus construct a phase diagram in the experimentally explored (Oh, We)-plane, which is shown on figure 6. The experimentally accessible plane is divided into four parts, where the main mechanisms at work during the impact process are different. These four parts are separated by the curves $Oh = 0.05$ and $We = Oh^{-4/3}$. They are labelled. as follows. IC-CI: the drop dynamics is given by a competition between inertia and capillarity both for the spreading and the retraction. IV-CV: inertia and viscous forces dominate the spreading, capillary and viscous forces dominate the retraction. These two regimes have been studied in detail here. The two more intriguing regions are IV-CI (viscous spreading, inertial retraction) and IC-CV (capillary spreading, viscous retraction) that are difficult to explore in detail. For the IV-CI regime, the large inertia at impact, combined with a small surface tension, will make the droplets undergo large non-axisymetric deformations and they will eventually splash and disintegrate. At the other

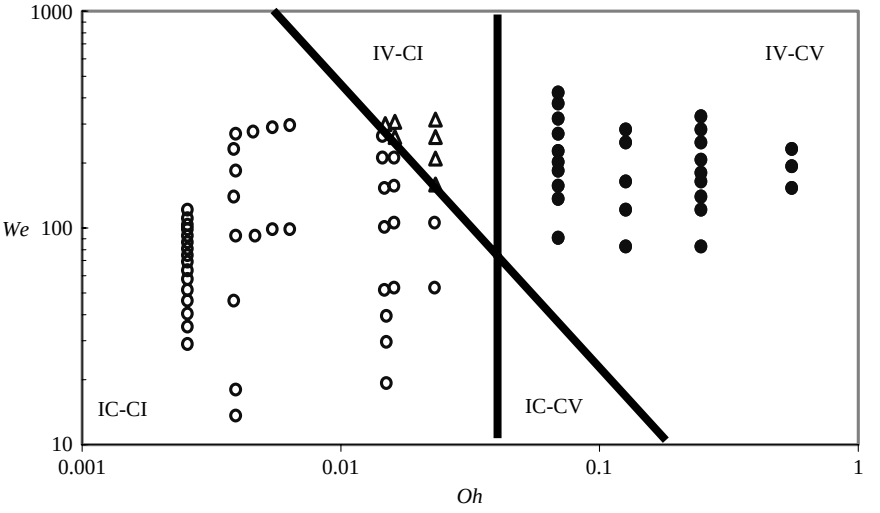

FIGURE 6. Phase diagram in the (We, Oh)-plane for the impact and retraction dynamics of droplets. The four regions are discussed in the text, and the symbols represent the parameters of the data reported in this paper. Different symbols have been assigned for each region.

end of the phase diagram, the IC-CV region corresponds to very low impact speeds and important capillary forces, implying very small deformations of the droplets. If the deformations are small, pinning of the contact line of the droplets will become important, and our simple scaling arguments for both the maximum radius and the retraction rate are invalidated.

A numerical investigation of droplet impact would be very helpful for two reasons. First, numerics would allow R_I to be varied while keeping all the other physical parameters constant. This would allow the robustness of our results to be checked, since experimentally it is not easy to vary R_I over a wide range. Second, as emphasized above, the viscous regime for the maximum radius is difficult to characterize precisely due to the smallness of the variation of R_{max} for viscous drops. If precise numerical simulations could be done, these different remaining problems could be resolved.

In sum, we have studied the retraction dynamics of liquid droplets upon high-speed impact on non-wetting solid surfaces. Perhaps the strongest conclusion from our investigation is that the rate of retraction of the droplet is a constant which does not depend on the impact velocity. Two regimes for the retraction rate have been identified: a viscous regime and an inertial regime. We have in addition shown here that simple hydrodynamic arguments can be formulated that give very reasonable agreement with experiments in the two different regimes.

Benjamin Helnann-Moussa is acknowledged for help with the experiments. Denis Bartolo is indebted to the CNRS for providing a post-doctoral fellowship. LPS de l'ENS is UMR 8550 of the CNRS, associated with the universities Paris 6 and Paris 7.

REFERENCES

BERGERON, V., BONN, D., MARTIN, J.-Y. & VOVELLE, L. 2000 Controlling droplet deposition with polymer additives. *Nature* **405**, 772–775.

BUGUIN, A., VOVELLE, L. & BROCHARD, F. 1999 Shock in inertial dewetting. *Phys. Rev. Lett* **83**, 1183–1186.

Clanet, C., Béguin, C., Richard, D. & Quéré, D. 2004 Maximal deformation of an impacting drop. *J. Fluid Mech.* **517**, 199–208.

Culick, F. E. C. 1960 Comments on a ruptured soap film. *J. Appl. Phys.* **31**, 1128.

Edgerton, H. & Killian, J. 1954 *Flash*. Charles T. Brandford Company, Boston.

Fukai, J., Zhao, Z., Poulikakos, D., Megaridis, C. M. & Miyatake, O. 1993 Modeling of the deformation of a liquid droplet impinging upon a flat surface. *Phys. Fluids* A **5**, 2588–2599.

de Gennes, P. G. 1985 Wetting: statics and dynamics. *Rev. Mod. Phys.* **57**, 827.

Mundo, C., Sommerfeld, M. & Tropea, C. 1995 Droplet-wall collisions: Experimental studies of the deformation and breakup process. *Intl J. Multiphase Flow* **21**, 151.

Okumura, K., Chevy, F., Richard, D., Quéré, D. & Clanet, C. 2003 Water spring: A model for bouncing drop. *Europhys. Lett.* **62**, 237–243.

Rein, M. 1993 Phenomena of liquid drop impact on solid and liquid surfaces. *Fluid Dyn. Res.* **12**, 61.

Richard, D., Clanet, C. & Quere, D. 2002 Contact time of a bouncing drop. *Nature* **417**, 811–811.

Roisman, I., Riboo, R. & Tropea, C. 2002 Normal impact of a liquid drop on a dry surface: model for spreading and receding. *Proc. R. Soc. Lond.* A **458**, 1411–1430.

Taylor, G. I. 1959 The dynamics of thin sheets of fluid iii. disintegration of fluid sheets. *Proc. R. Soc. Lond.* A **253**, 253–313.

Ukiwe, C. & Kwok, D. Y. 2004 On the maximum spreading diameter of impacting droplets on well-prepared solid surfaces. *Langmuir* **21**, 666–673.

Worthington, A. 1876 On the form assumed by drops of liquids falling vertically on a horizontal plate. *Proc. R. Soc. Lond.* **25**, 261–271.